Manta Ray inspired multistable soft robot

Juan C. Osorio¹, Chelsea Tinsley¹, Kendal Tinsley¹ and Andres F. Arrieta¹

Abstract - Manta rays are unique animals that exhibit complex motion behavior, given their rigid bodies and flexible fins. During turning maneuvers, these animals can hold their fins in asymmetric positions while flapping to achieve a smaller turning radius and faster-turning speed. This collective behavior can be challenging to attain using conventional soft robots or actuators. Local bistability can be leveraged to mimic this behavior by inducing spatially distributed prestress in thin, fin-like surfaces that reshape into 3D, stable configurations without the need of continuous actuation. We present a pneumatically actuated manta ray-inspired soft robot concept with multiple stable states which approximate the ray's asymmetric strokes and stroke frequency. The fins are actuated by an array of inflatable bistable and metastable dome-shaped units that allow us to independently deflect sections of the fin to achieve a desired position. We tune our robot's geometry by performing a numerical parameter sweep over different geometrical configurations of the patterned dome structure. Our approach offers a new route for imposing various target 3D deflected positions of morphing surfaces with minimal actuation or feedback control by utilizing multistability.

I. INTRODUCTION

Manta rays display several morphological and kinematic traits that are advantageous in bioinspired robot design. These animals are classified as rigid-bodied as they are relatively rigid about the longitudinal axis (along the spine) [1]. Since most robots incorporate rigid components, it is typically easier to mimic rigid-bodied animals than their soft-bodied, longitudinally-flexible counterparts. De-spite soft-bodied aquatic animals generally achieving supe-rior maneuverability-to-size ratios, manta rays perform at the peak ability of rigid-bodied fish and achieve performance levels that rival those of soft-bodied fish [1]. Moreover, manta rays are incredibly energy-efficient, making them an ideal model for long-distance, untethered robots. For instance, manta rays have been found to possess a Froude efficiency of 48% [2], comparable to that of the flexible-bodied trout. Manta rays also far exceed the 34% Froude efficiency of stingrays, which are a similar, rigid-bodied animal.

Several approaches have been taken to design manta rayinspired robots. Broadly, these designs are capable of one or more of the following types of fin control: 1) spanwise control (out from the body), 2) chordwise control (along the length of the body), and/or 3) surface stiffness control. In general, achieving more fin control requires more actuation complexity, as illustrated in Fig.1a. Wang Z, Wang Y, Li J et al. [3] demonstrated chordwise control by using a single active spar on the leading edge of the pectoral fin. While this design required minimal control, it also reduced the nuances of the fin structure. Thus, a forward motion of the robot was achieved, but maneuverability was limited. More spars can be added along the length of the body to increase control of the fin's geometry. Having multiple spanwise spars allows the chordwise fin geometry to be varied, allowing improved maneuverability without sacrificing forward thrust capabilities. For example, Yang et al. [4] demonstrate that their manta ray robot can perform pivot turning. Other studies have shown spanwise fin control by connecting rigid chordwise segments with hinges [5]. With only spanwise fin control, the pectoral fin can closely follow the amplitude of a manta ray's flapping motion. However, forward thrust cannot be achieved effectively, which is impractical for an aquatic robot.

Moreover, rigid hinged segments can be applied in both the chordwise and spanwise directions to gain forward thrust while achieving significant control of the spanwise fin profile [6], mimicking the complex bone structure [7] of a manta ray's pectoral fins. However, this requires an intricate fin structure with many components and a complex control system. An alternative approach to accurately capture the fin's complex deflecting geometry in both the chordwise and spanwise directions is fabricate the fin from a continuous flexible material instead of individual rigid linkages. Suzumori et al. [8] achieved this using a silicone fin of varying thickness. The variable thickness allows for fin sections to exhibit different stiffnesses. Thus, the complex fin geometry can be closely matched even using simple control, such as single actuation along the leading ridge of the fin. However, as only the leading edge is powered, this fin design cannot generate significant forward thrust, limiting its capabilities. Chordwise, spanwise, and fin stiffness control can be achieved together, but often at the cost of added actuation complexity. Hao et al. [9] reached a high level of fin shape control by using carbon fiber spars of varying thicknesses to tailor the stiffness of the fin. The spars are angled back and outboard, allowing for coupled chordwise and spanwise control of the fin. However, each spar must be controlled by a separate servo actuator, resulting in a complex actuation system and large part count.

This work presents a manta ray-inspired robot concept combining soft materials with bistable structures. By merging these elements, our robot can reach and lock at different fin configurations (set points). It uses the energy released during snap-through of dome-shaped bistable elements to trigger local reconfiguration of the fin for controlled bursting at each set point. Specifically, we leverage the local deflections

^{*}This work is supported NSF CAREER grant No. 1944597

¹School of Mechanical Engineering, Purdue University, West Lafayette
IN, USA aarrieta@purdue.edu

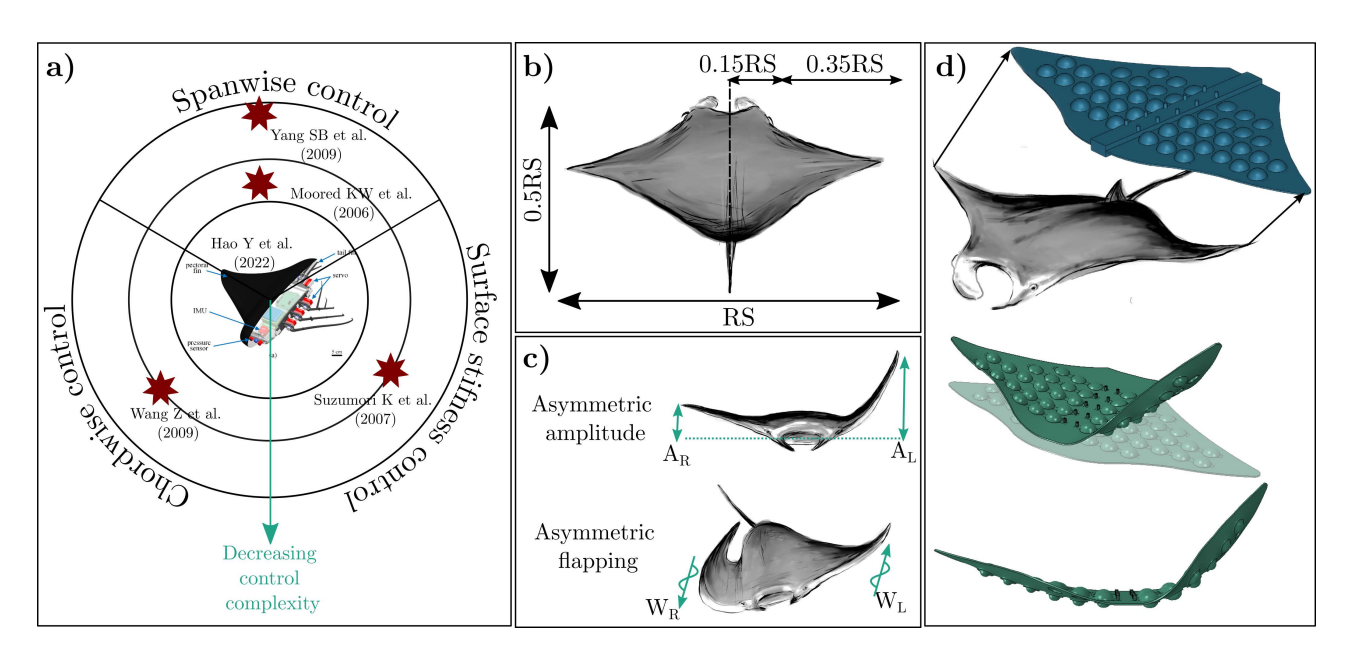


Fig. 1. Manta ray inspired soft robotics, control complexity, and multistable soft manta ray concept. a) Current manta ray-inspired soft robots. Types of control and control complexity. b) General dimension of Manta Rays in terms of manta ray span (RS) c) General Ray behavior during turning maneuvers (Asymmetric amplitude (A_R and A_L) and phase difference for forward trust (Bursting) (W_R and W_L) [9]. d) Ray-inspired multistable soft robot concept and different stable shapes.

induced by the inversion of the bistable domes to reconfigure into a desired shape (set point) about which the fin oscillates due to the kinetic and strain energy exchange. The induced fin oscillations allows us to mimic the stereotypical fin bursts that mantas display during sharp, powered turns. The robot was designed using the Finite Element Method (FEM), by performing a parameter sweep over different geometrical configurations of the dome structure and evaluating the effect on the robots' fins. The final bistable domes' was selected by determining the best geometric parameters that approximate the robot's desired fin topography and bursting behavior. Finally, we qualitatively validated our results by 3D printing the final shape using thermoplastic polyurethane (TPU) and comparing the system's experimental and theoretical programmed stable shapes.

II. MANTA RAY BEHAVIOR

Manta rays are capable of several locomotion forms, including forward propulsion (swimming), unpowered turns (banking), and powered turns (bursting). In order to match the manta ray's propulsive and turning performance, a robot must be able to attain the spanwise and chordwise topology and stiffness of the pectoral fins during these maneuvers. In an unpowered turn, the lift force is generated normal to the fin's upper surface. By banking steeply, the lift vector is pointed towards the inside of the turn, generating radial force that allows the manta to turn. To perform this maneuver, the banking angle must be between 65 to 70 degrees from horizontal, and the pectoral fins must be held in a dihedral position [1]. When performing a powered turn, the manta rays use banking to create radial force and asymmetric fin strokes (see Fig. 1c) to generate torque about the body's center. This allows them to achieve a smaller turning radius

and higher turning velocity. The flapping sequence during a turn includes a swimming stroke and a gliding portion, where the glide occurs when the fins are at the top of the upstroke amplitude. The outboard fin stroke amplitude is 1.7±0.6 times the amplitude of the inboard stroke [1] (see Fig. 1c A_L/A_R). While the fin's position and angle during turning maneuvers are not well characterized, metrics of position vs. time for turning can be derived from data from Fish et al. [2] on the position and angle of the fins during straight swimming. Points of interest include the fin's tip and a point halfway between the root and the tip. At these positions, Fish et al. report that the fin's vertical displacement during the upstroke reaches a maximum of about 65% and 20% of the body length, respectively. These points provide a target desired design geometry for the inboard fin. We use the fin amplitude vs. time data from Fish et al. [2], introducing appropriate scaling to serve as the position metrics of the fin's programmed shape during a powered turn. Similarly, we use the reported pitch angle vs. time to develop the angle metrics for the programmed shapes. Since the gliding motion occurs at the top of the stroke, the position and angle metrics at the top are also used as the metrics for an unpowered gliding turn.

While accurately matching the manta ray's fin positions and angles through a maneuver can allow the robot to roughly follow the desired path, the stiffness of the pectoral fins must also be met to achieve the efficiency and precision of the manta ray [11]. Schaefer and Summers's [11] investigations of the pectoral fins' bone and cartilage structure indicate that the fins have great flexibility throughout their span. However, the chordwise stiffness is increased along the fin's root and leading edge to support the normal forces created during powered strokes. The chordwise and spanwise

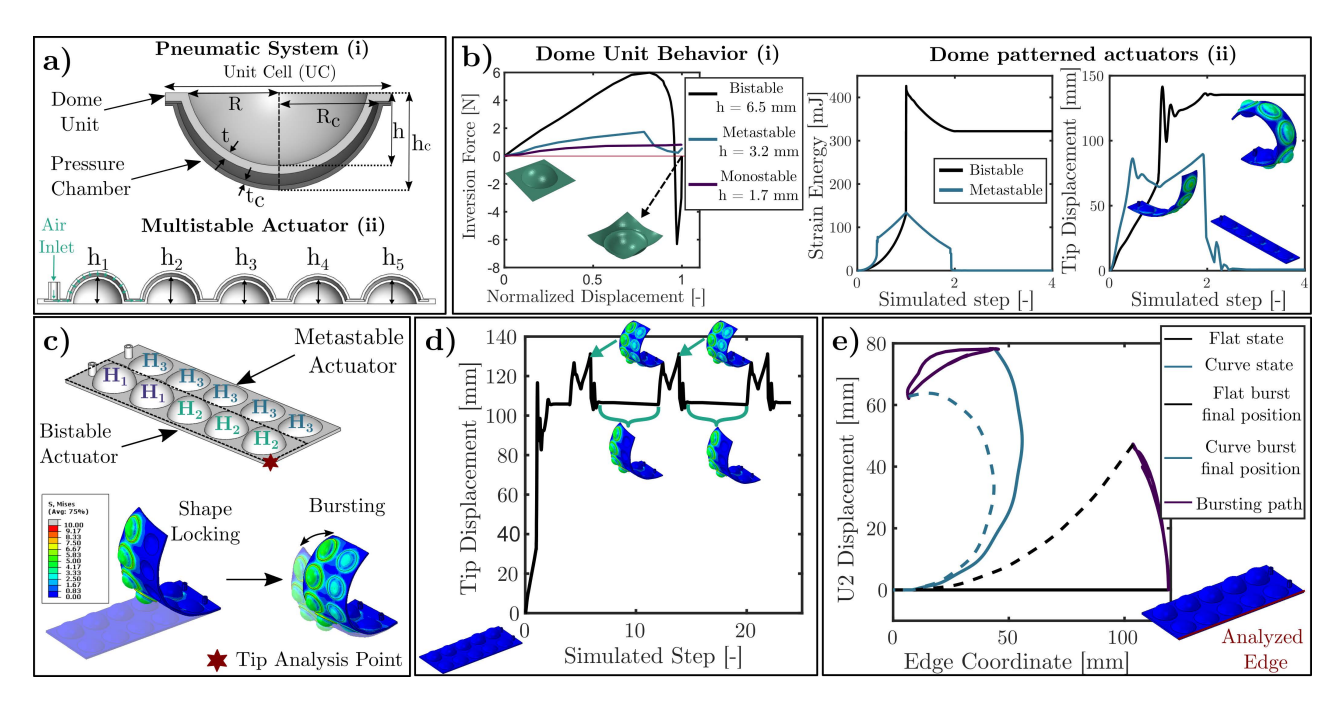


Fig. 2. Multistable soft actuators with shape locking and bursting capabilities. a) Actuator geometry and influence of dome geometric parameters on its mechanical response. (i) Dome unit pressure chamber for pneumatic actuation [10], (ii) Pattern array of units with different heights (h_1 to h_5) to form a multistable actuator. b) (i) Unit cell mechanical response for different dome heights bistable ($h_1 = 6.5$ mm), metastable ($h_2 = 3.2$ mm), and monostable($h_1 = 1.7$ mm) Force vs. Displacement plots. (ii) FE simulation of a five dome-unit bistable ($h_1 = h_2 = h_3 = h_4 = h_5 = 6.5$ mm) and metastable ($h_1 = h_2 = h_3 = h_4 = h_5 = 3.2$ mm) row actuator. c) Doble row combined bistable+metastable actuator and its expected locking and bursting behavior ($H_1 > H_2 > H_3$). d) Combine actuator tip displacement over time. Shape locking on the system's stable state (set point) and bursting in that given state. e) Bursting path in two different stable states (Flat and curved state). Bursting occurs as the domes in the metastable region are inverted.

flexibility along the trailing edge of the fins allows an increase in propulsive efficiency and is therefore desirable to apply to the robot manta ray [2].

III. MULTISTABLE ACTUATORS

To replicate manta rays' complex movements and unique fin properties, we utilized structural multistability to develop surfaces that can morph using a pneumatically actuated matrix of domes on its surface. Each dome unit cell is composed of two shells, where the inner dome buckles outward when the space between them is inflated (unit cell and pressure chamber shown in Figure 1 a(i)). This topology [10] allows the dome's state to be switched between the asmanufactured (ground) and inverted (stressed) states (Figure 2b (i)). Using patterned arrays of these units and tailoring their local mechanical response, we can create a unique global shape reconfiguration that approximates the ray's asymmetric fin stroke amplitude and bursting movement.

FE simulations of the soft actuators and soft robots were performed using the commercial software ABAQUS. We utilize a 3D geometry of each domain to capture the activation path of the structures. Every domain was meshed with C3D10 tetrahedral elements with an average element size of 1.5 mm for the surface and 0.2 mm for the thickness. A nonlinear quasi-static dynamic implicit analysis is implemented to consider each dome's snap-through instability and improve the simulation's convergence. The system's stability is guaranteed by applying constant pressure in each unit and adding several relaxing steps to release the activation

energy. Ultimaker TPU 95A using a linearly elastic material model with isotropic Young's modulus of E=26 MPa is used in the simulations. Given the nature of the actuation system, dynamic analysis and inertial terms are necessary to capture the structure's full actuation path, predict different stable shapes, and the oscillatory bursting response.

Dome Unit Shape: The dome shape unit is a semi-spherical geometry that can be characterized using geometrical by the dome height (h), thickness (t), internal radius (R) and Unit Cell (UC) size (see Figure 2a (i)). Each geometric parameter modifies the mechanical response of the unit cell, making it exhibit monostability, metastability, or bistability [12] (Fig. 2b (i)). Every unit can be snapped using a pneumatic actuation system (Fig. 2a (i)). The domelike air chamber has the same dome unit thickness (t = t_c) but increased dome radius and height dimensions ($t_c = t_c$) mm and $t_c = t_c$ mm. We selected this geometry for the actuation system based on our previous work [10], which was developed to decrease the 3D printing complexity.

Soft Actuators / Dome Rows: Dome row actuators (Fig. 2a (ii)) are composed of an array of dome-shape units. By selecting the appropriate geometrical parameters, the units can be locally bistable causing the row to exhibit global curvature and a stable position after all units are inverted [12, 13]. As each dome unit can be tailored geometrically to have different stable points (see Fig. 2b (i)), row actuators can be designed to achieve multiple stable states with a single pressure input. As different dome heights (i.e., h_1 , h_2 , h_3 , h_4 , and h_5) require different inversion pressures, the dome row

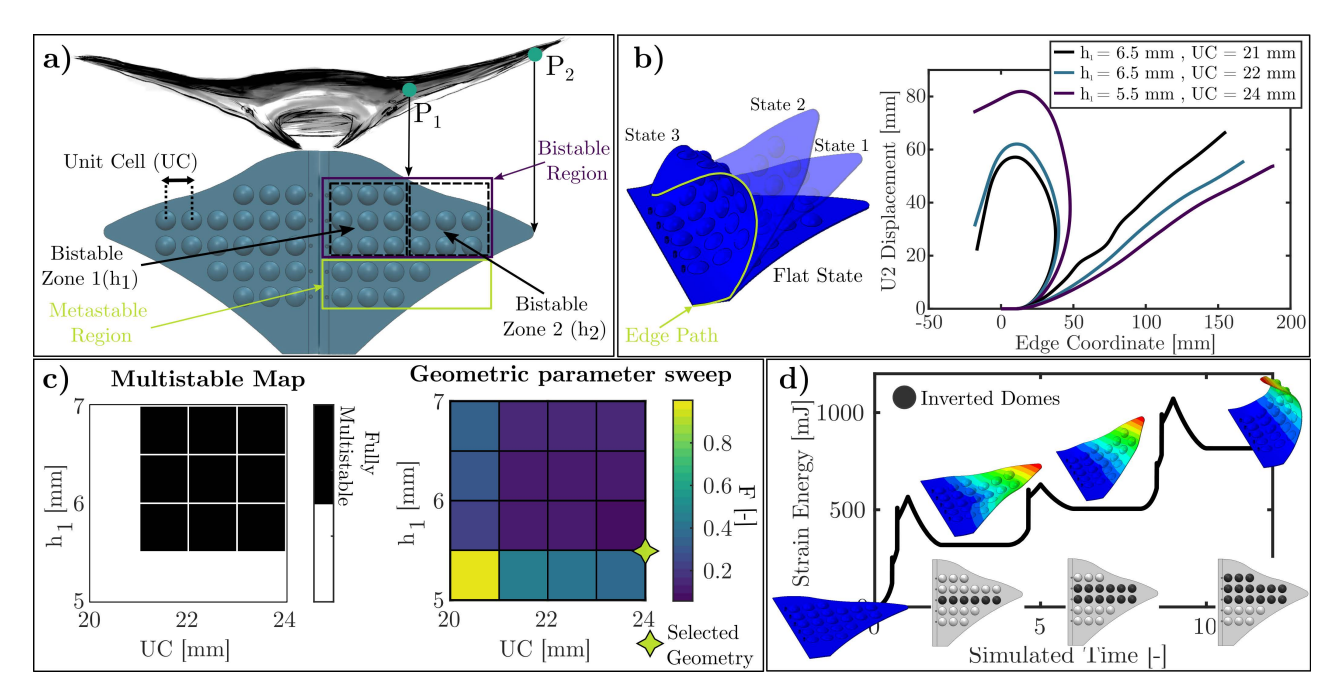


Fig. 3. Manta Ray inspired design and behavior. a) Geometric parameters of multistable fin inspired by manta ray body. Bistable (Dome height $h_1 > h_2$) and metastable zones within the fin and targeted shape points (P_1 and P_2). b) Obtained stable states with the proposed robot topology and the effect of bistable zone 1 height (h_1) and Unit cell (UC) size on different stable shapes. c) Multistable map and geometric parameter sweep over different values of bistable zone 1 height (h_1) and Unit cell size (UC). Selected geometry is chosen from minimum values of F and a fully multistable system. d) Stable states of the selected geometry and its multiple energy minima after individual row inversion. Three different stable energy levels can be observed.

can be altered to have as many stable states as geometrically unique bistable dome units, thus achieving fine spatial control without colocated actuators. Instead, pressure modulation over time plays the role of local actuators allowing to realize complex spatial reconfiguration. We ilustrate this by selecting different heights that guarantee bistability, we can create an actuator with two distinct shapes: a flat stress-free shape and a curved inverted shape, as shown by the changed tip position in Fig. 2b (ii). This shape change is achieved by retaining the strain energy within the structure (Fig. 2b (ii) strain energy plot), which comes from every local dome inversion. Moreover, we can select geometrical parameters to exhibit metastable properties (see Fig. 2b(i)) [12], which means that the unit exhibits snap-through, releasing strain energy in the process, but returns to its original shape once the external force is removed [14]. Leveraging their collective behavior yields a metastable actuator (Metastable in Fig. 2b (ii)), that oscillates due to snap-through and snap-back cycles that store and release strain energy. As shown in previous works [15, 16], the strain energy released during the snapthrough can be utilized as a simple bursting mechanism for locomotion.

Combining Soft Actuators: The full potential of these multistable actuators can be achieved by combining both the bistable and metastable topologies (see Fig. 2c). By incorporating both mechanical responses in the system, we can target a desired stable position (Shape locking Fig. 2c) and oscillate about it by using the bursting motion generated by actuating the metastable units (Bursting Fig. 2c). This gives the actuator the unique capability of having different

set points as stable states of the structure about which it can oscillate. These stable positions are embedded in the system's geometrical features and mechanical response, providing reconfiguration capability and adding actuation functionality in the neighborhood of the set point. The combined system consists of two 5-dome actuators with three different dome heights (H_1 , H_2 , and H_3 in Fig. 2c). The bistable actuator consists of two dome classes with heights H_1 = 6.5 mm and H_2 = 7.5 mm, respectively. We selected the heights to have different curvatures along the actuator length. For the metastable actuator, we chose a dome height of H_3 = 3.15 mm and individual air inlets to have independent control over each actuator. Both actuators are modeled with t = 0.75 mm, R = 8 mm, and unit cell size UC = 22 mm (see Fig. 2a).

Combining these two actuators can achieve shape-locking capabilities and a bursting motion about the programmed stable shapes. By shape-locking the structure, we can achieve large fin deflections, and by utilizing the bursting motion, we can perform the power turn while the fins are locked in the optimal position. We further demonstrate the system's capabilities by examining the tip displacement for different simulated actuation steps. Results show that the structure returns to the locked shape once the metastable actuator resets itself. This expands the versatility and capabilities of the system, as it can burst at any given stable shape, as demonstrated for the flat and curve state in Fig. 2e. The combined effect of the actuator can be leveraged to replicate some of the most complicated movements that manta rays perform during power turns.

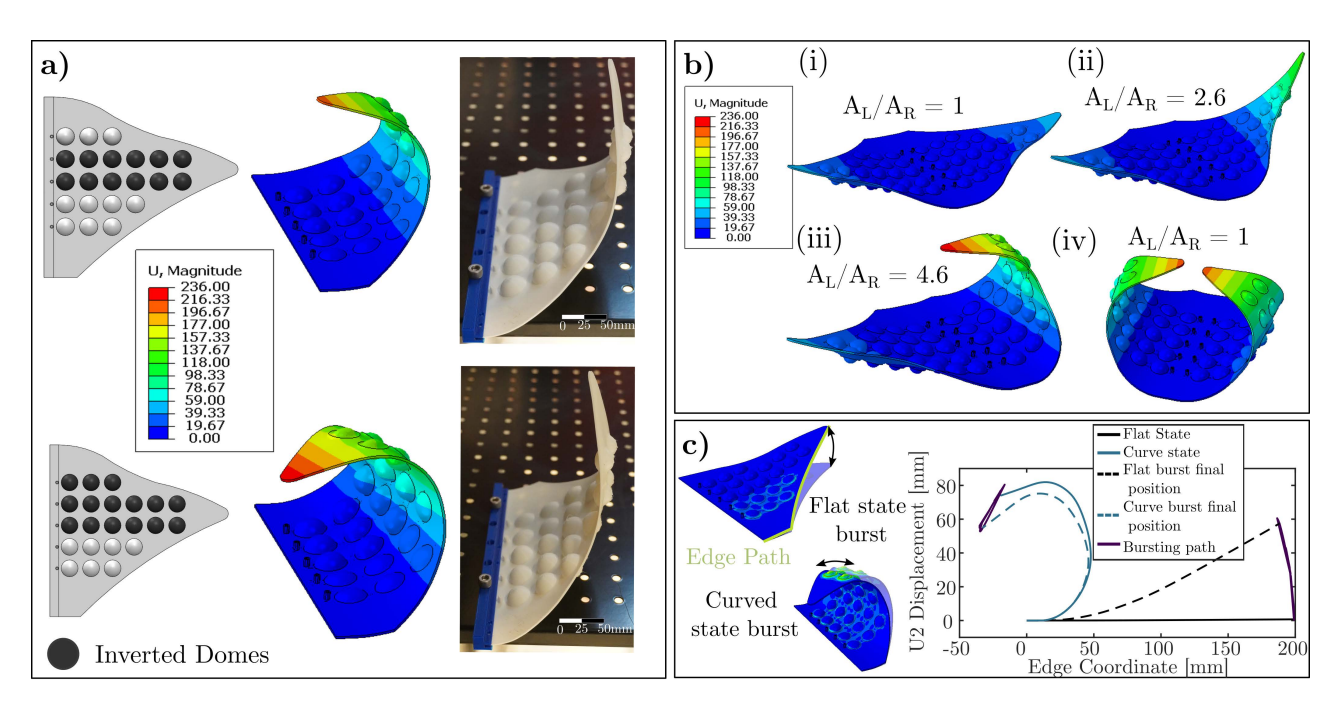


Fig. 4. Fin performance and full manta ray stable states. a) Qualitative comparison between different soft fin stable states found experimentally and numerically (FE). b) Asymmetric stroke is reached when two fins are joined to form the full manta ray body. Different A_L/A_L relations depend on the number of active domes. c) FE simulation of the bursting motion of the fin at two different stable points (Flat and curved states). Bursting path and edge path positions during bursting for the flat and curve state.

IV. MATCHING AND LOCKING OF FIN SHAPES

Inspired by the manta ray's complex behavior and the combined actuator's capabilities, we propose a soft robot approximating the manta ray's global morphology (Fig. 3a). We based our design and dimensions on previous studies [17] illustrated in Fig. 1b. Given its symmetry along its longitudinal axis, the robot design and overall performance tests are conducted by analyzing just half of the manta ray (soft fin). The fin is composed of two regions, bistable and metastable (see Fig. 3a) zones, where dome row actuators are utilized to achieve specific functionalities (see Section III for details). We selected three bistable row actuators to increase the final curvature of the fin once all dome units are inverted in the bistable region. By selecting this configuration, our geometry exhibits three stable shapes for every combination of active actuators.

The fin's bistable region is divided into two different zones, which are differentiated by the dome height (h_1 and h_2), allowing it to adopt different curvatures along the span. Moreover, we included two metastable row actuators in the bottom part of the fin (metastable zone in Fig. 3a) to obtain the combined response (section III) that matches a global geometry while allowing for bursting motion bout each stable configuration. Given the multiple geometric parameters and their influence on the final shape of the fin (see Fig. 3b), we performed a parameter sweep to determine the best geometry that matches the manta ray shape. The unit cell (UC) size and dome high on bistable zone 1 (h_1) are selected as our design parameters, which are explored between (20 mm -24 mm) and (5 mm - 7 mm), respectively. The height on bistable zone 2 (h_2) was set to be $h_1 + 1$ mm, while the

rest of the parameters remained constant with the values already mentioned in section III and illustrated in Fig. 3a. Two different analyses are performed using finite element (FE) simulations. First, a multistable analysis, as some given geometries generate high interaction between dome units which impede the ability to invert all domes simultaneously. We discard geometries showing that behavior as they do not guarantee locking capabilities and predictable, stable shapes. The analyzed geometries are labeled as Fully Multistable in the multistable map shown in Fig. 3c. Each parameter combination is tested by comparing the final state after all bistable actuators are activated, against the manta's fin amplitude at two different points. We use a performance criterion stating the stroke amplitude about selected points along the fin's span, given by:

$$F = \frac{1}{RS} ((0.3RS - P_2) + (0.15RS - P_1))$$
 (1)

Where RS is the total manta ray's span (Fig. 1b), and P_1 and P_2 correspond to the amplitude of the stroke at those specific points. For the selected P_1 and P_2 points, the stroke amplitude needs to be 0.15RS and 0.3RS, respectively [2]. The value of F for different UC and h_1 can be observed in Fig. 3c, where the minimum value (indicating the closest match) corresponds to h_1 = 5.5 mm and UC = 24 mm. Fig. 3d shows the resulting fin set points achieved by inverting different bistable dome rows. A qualitative comparison between the stable states found numerically and experimentally was performed for the final fin design (i.e., with parameters h_1 = 5.5 mm, h_2 = 6.5 mm, and UC = 24 mm). Fig. 4a shows two different existing stable states on the 3D-printed fin. The

experimental tests show that the fin's curvature increases each time one bistable actuator is activated, qualitatively matching the observed behavior from FE simulations. The main differences between the numerical and the experimental specimen's shapes result from neglecting gravity in our computational analysis.

V. MULTISTABLE SOFT MANTA RAY ROBOT

We implemented a multistable manta ray robot by combining two soft fins (see Fig.4.b). We examine the fins' combined behavior by activating a different set of bistable row actuators to achieve asymmetric stroke amplitudes. Fig. 4b shows the numerical results obtained for different active rows revealing the robot's ability to reach and retain the desired asymmetric position. We measure the ratio between the right fin amplitude (A_R) and the left fin amplitude (A_L), which is relevant for mimicking the ray's behavior (see section II for details). We report the obtained configurations and their A_L/A_R ratio in Fig 4b, showing that a 4.7 times difference between both fins is achievable.

A final numerical analysis is performed by locking the fin in two different stable positions (i.e., flat and curved/fully activated) and inverting the metastable actuators to generate bursting motion around the two set points. FE results show that this actuation method can obtain motion between two states, with an amplitude of 0.1RS for the flat state and 0.05RS for the fully active state (see Fig 4c). This indicates that the energy released during the snap-through of the metastable region can generate bursting motion about programmed stable positions.

VI. CONCLUSIONS AND FUTURE WORK

A soft robot leveraging structural multistability is presented to approximate the complex shape morphing of manta rays. Bistable and metastable soft row actuators are utilized to replicate these mantas' fin-locking and fin-bursting capabilities during power turns. The mechanics of multistable surfaces allow us to introduce unique functionalities in our fin structure by changing the geometrical features of our dome-shaped unit. We demonstrate the ability to program different stable configurations and ranges of motion into a topology analogous to a manta ray fin. We design the fin topology to match specific stroke amplitudes in the tip and middle section of the fin by performing a parameter sweep over the unit cell size and dome height. Finally, a qualitative experimental comparison was performed, showing the resemblance between the predicted stable states and a physical 3D-printed fin. We demonstrate that by incorporating tailored metastable row actuators, oscillation from snap-through instability can be achieved around stable states, which can generate bursting-like motions. The obtained results indicate the capabilities of the proposed design and an approach to leverage multistability for both shape locking and underwater bursting. Our work illustrate the potential of adopting bistable and metastable structures to simplify complex motions from shape reconfiguration shown by organisms, which can be used to attain better-performing

underwater robots. Future work will focus on establishing an optimization method to target different fin stroke amplitudes and dynamic bursting motions enabling both control and propulsion.

ACKNOWLEDGMENTS

We acknowledge the support of the NSF-CAREER award No. 1944597. In addition, authors would like to acknowledge Valentina Castañeda for her contributions on the manta ray schematics.

REFERENCES

- [1] F. E. Fish, A. Kolpas, A. Crossett, M. A. Dudas, K. W. Moored, and H. Bart-Smith, "Kinematics of swimming of the manta ray: Threedimensional analysis of open-water maneuverability," Journal of Experimental Biology, vol. 221, no. 6, 3 2018.
- [2] F. E. Fish, C. M. Schreiber, K. W. Moored, G. Liu, H. Dong, and H. Bart-Smith, "Hydrodynamic Performance of Aquatic Flapping: Efficiency of Underwater Flight in the Manta," Aerospace 2016, Vol. 3, Page 20, vol. 3, no. 3, p. 20, 7 2016.
- [3] Z. Wang, Y. Wang, J. Li, and G. Hang, "A micro biomimetic manta ray robot fish actuated by SMA," in 2009 IEEE International Conference on Robotics and Biomimetics, ROBIO 2009, 2009, pp. 1809–1813.
- [4] S. b. Yang, J. Qiu, and X. y. Han, "Kinematics Modeling and Experiments of Pectoral Oscillation Propulsion Robotic Fish," Journal of Bionic Engineering, vol. 6, no. 2, pp. 174–179, 6 2009.
- [5] K. W. Moored, S. A. Taylor, T. K. Bliss, and H. Bart-Smith, "Optimization of a tensegrity wing for biomimetic applications," in Proceedings of the 45th IEEE Conference on Decision and Control, 2006, pp. 2288–2293.
- [6] R. S. Russo, S. S. Blemker, F. E. Fish, and H. Bart-Smith, "Biomechanical model of batoid (skates and rays) pectoral fins predicts the influence of skeletal structure on fin kinematics: implications for bioinspired design," Bioinspiration & Biomimetics, vol. 10, no. 4, p. 046002, jun 2015.
- [7] Y. Lu, Y. Cao, G. Pan, Q. Huang, X. Dong, and Y. Cao, "Effect of Cross-Joints Fin on the Thrust Performance of Bionic Pectoral Fins," Journal of Marine Science and Engineering, vol. 10, no. 7, 7 2022.
- [8] K. Suzumori, S. Endo, T. Kanda, N. Kato, and H. Suzuki, "A bending pneumatic rubber actuator realizing soft-bodied manta swimming robot," in Proceedings 2007 IEEE International Conference on Robotics and Automation, 2007, pp. 4975–4980.
- [9] Y. Hao, Y. Cao, Y. Cao, Q. Huang, and G. Pan, "Course Control of a Manta Robot Based on Amplitude and Phase Differences," Journal of Marine Science and Engineering, vol. 10, no. 2, 2 2022.
- [10] J. C. Osorio, H. Morgan, and A. F. Arrieta, "Programmable Multistable Soft Grippers," 2022 IEEE 5th International Conference on Soft Robotics, RoboSoft 2022, pp. 525–530, 2022.
- [11] J. T. Schaefer and A. P. Summers, "Batoid wing skeletal structure: Novel morphologies, mechanical implications, and phylogenetic patterns," Journal of Morphology, vol. 264, no. 3, pp. 298–313, 6 2005.
- [12] J. A. Faber, J. P. Udani, K. S. Riley, A. R. Studart, and A. F. Arrieta, "Dome-Patterned Metamaterial Sheets," Advanced Science, vol. 7, no. 22, 11 2020.
- [13] J. P. Udani and A. F. Arrieta, "Programmable mechanical metastructures from locally bistable domes," Extreme Mechanics Letters, vol. 42, p. 101081, 1 2021.
- [14] Y. Chen, T. Liu, and L. Jin, "Spatiotemporally Programmable Surfaces via Viscoelastic Shell Snapping," Advanced Intelligent Systems, vol. 4, no. 9, p. 2100270, 9 2022.
- [15] Y. Chi, Y. Li, Y. Zhao, Y. Hong, Y. Tang, J. Yin, Y. Chi, Y. Li, Y. Zhao, Y. Hong, J. Yin, and Y. Tang, "Bistable and Multistable Actuators for Soft Robots: Structures, Materials, and Functionalities," Advanced Materials, vol. 34, no. 19, p. 2110384, 5 2022.
- [16] Y. Chi, Y. Tang, H. Liu, and J. Yin, "Leveraging Monostable and Bistable Pre-Curved Bilayer Actuators for High-Performance Multitask Soft Robots," Advanced Materials Technologies, vol. 5, no. 9, p. 2000370. 9 2020.
- [17] K. H. Low, C. Zhou, G. Seet, S. Bi, and Y. Cai, "Improvement and testing of a robotic Manta Ray (RoMan-III)," 2011 IEEE International Conference on Robotics and Biomimetics, ROBIO 2011, pp. 1730– 1735, 2011.